Controlling the Most Significant Grating Lobes in Two-Dimensional Beam-Steering Systems with Phase-Gradient Metasurfaces

Khuhsboo Singh, *Student Member, IEEE,* Muhammad U. Afzal, *Member, IEEE,* Maria Kovaleva, *Student Member, IEEE,* and Karu P. Esselle, *Fellow, IEEE*

***Abstract*—High-directivity antenna systems that provide 2D beam steering by rotating a pair of phase-gradient metasurfaces in the near field of a fixed-beam antenna, hereafter referred to as Near-Field Meta-Steering systems, are efficient, planar, simple, short, require less power to operate and do not require antenna tilting. However, when steering the beam, such systems generate undesirable dominant grating lobes, which substantially limit their applications. Optimizing a pair of these metasurfaces to minimize the grating lobes using standard methods is nearly impossible due to their large electrical size and thousands of small features leading to high computational costs. This paper addresses this challenge as follows. Firstly, it presents a method to efficiently reduce the strength of "offending" grating lobes by optimizing a supercell using Floquet analysis and multi-objective particle swarm optimization. Secondly, it investigates the effects of the transmission phase gradient of PGMs on radiation-pattern quality. It is shown that the number of dominant unwanted lobes in a 2D beam-steering antenna system and their levels can be reduced substantially by increasing the transmission phase gradient of the two PGMs. This knowledge is then extended to 2D beam-steering systems, where we demonstrate how to substantially reduce all grating lobes to a level below -20 dB for all beam directions, without applying any amplitude tapering to the aperture field. When steering the beam of two Meta-Steering systems with peak directivities of 30.5 dBi and 31.4 dBi, within a conical volume with an apex angle of 96°, the variation in directivity is 2.4 dB and 3.2 dB, respectively. We also demonstrate that beam-steering systems with steeper gradient PGMs can steer the beam in a wider range of directions, require less mechanical rotation of metasurfaces to obtain a given scan range and their beam steering is faster. The gap between the two metasurfaces in a Near-field Meta-Steering system can be reduced to one-eighth of a wavelength with no significant effect on pattern quality.**

***Index Terms*—Near-field, phase transformation, beam-steering, high-gain antenna, phase gradient metasurfaces, lens antenna, transmitarray, meta-material, satellite communication, SATCOM, 5G, SOTM, COTM, Satellite TV, RLSA, EBG, sidelobe, SLL.**

I. Introduction

STEERING a highly directive antenna beam (with directivity $>$ 20 dBi) in two angular dimensions, i.e. in both elevation and azimuth planes, is one of the most challenging and widely researched topics in electromagnetic and antenna engineering. Such antenna systems are required in many current and emerging applications including mobile satellite communication, communication with non-geostationary satellites, networking of spacecrafts and space vehicles (Wi-Fi in Space) and reconfigurable wireless millimetre-wave relaying and backhauling of 5G cells and small cells. Steering such a beam in the elevation plane over a wide angular range while maintaining high directivity, a small beamwidth and low sidelobe levels is especially very challenging.

Nearly all current methods of wide-range two-dimensional (WR2D) high-directivity beam steering can be broadly classified into three Groups: Systems with (A) rotation and tilting; (B) rotation but no tilting; (C) fully electronic steering. Some hybrid combinations of these are also possible. Some examples for Group A are parabolic reflector antenna systems [1], [2] designed for defence vehicles for satellite communication [3] and for cruise ships for satellite TV reception. As the whole antenna is rotated and tilted when steering, these systems have excellent performance, but they are tall, bulky, heavy and require expensive heavy-duty motors. For providing internet to aeroplanes, the reflector antenna is replaced by a flat rectangular panel antenna (usually a horn array or waveguide array) to make the system shorter at the expense of increased beamwidth in the elevation plane and some beam distortion when the beam is tilted down closer to the fuselage [4].

There are fewer examples for Group B. Perhaps the most successful in aerospace industry is the Continuous Transverse Stub − Variable Inclination method [5], which requires three or more rotating antenna parts including a polariser. These systems are complex and expensive but have a much lower profile than Group A antenna systems. A more recent example for Group B is an antenna system based on near-field phase transformation in which two thin phase-gradient metasurfaces (PGMs), placed very close to the aperture of a base antenna that has a fixed beam, are rotated for 2D beam steering [6], [7]. This Near-Field Meta-Steering method is very flexible, and any antenna can be used as the base antenna, which is completely stationary. The two metasurfaces can be rotated using low-cost stepper or linear motors. Low profile, low power requirement (AC/DC), simplicity, high efficiency and low cost are the main advantages. In fact, the metasurfaces in such a system can also be placed several wavelengths (about 8-10 times wavelength) away from the base antenna (e.g. [8]) at the expense of low profile. In a very thin volume, a

Khushboo Singh and Muhammad U. Afzal are with the Centre for Collaboration in Electromagnetics and Antenna Engineering, School of Engineering, Macquarie University, Sydney, NSW 2109, Australia (e-mail: khushboo.singh@students.mq.edu.au). Maria Kovaleva is with ICRAR-Curtin, Curtin University, Perth, Australia. Karu P. Esselle is with School of Electrical and Data Engineering, University of Technology, Sydney, NSW 2007, Australia (karu.esselle@uts.edu.au).

WR2D Near-Field Meta-Steering to some extent mimics the operating mechanism of an optical Risely Prism system, which is many millions of wavelengths tall [9]–[11]. Some recent transmitarray or reflectarray systems with sliding or rotating metasurfaces are other examples for Group B [12], [13].

A phased array with electronic phase shifters is a well-known example for Group C. To achieve the high directivity required for satellite communication, several thousands of antenna elements and phase shifters are required, costing one particular antenna system approximately 1 million US dollars [14] and thus, limiting their application to the top end, such as expensive radar systems for defence applications. Their main advantage is speed [15]–[17]. Despite significant investment by several companies, a low-cost WR2D electronically-steered antenna system with high efficiency is yet to be realized.

Returning to metasurfaces, large aperture PGMs can be viewed as generalized reflectors and refractors, which produce spurious diffraction orders eventually generating periodic lobes [18]–[20]. The majority of recent research advances on metasurfaces has focused on achieving large offset tilting of a fixed input beam by introducing phase discontinuities. Only a few attempts have been made to obtain desired beam tilt while simultaneously maintaining low side-lobe levels (SLLs) [21]. Some attempts have been made to reduce scattering but without beam steering [22], [23]. It must be emphasized here that controlling the side lobes in a beam-scanning system is as vital as obtaining a large scan range. There has been no investigations so far, on how a pair of closely placed metasurfaces with large tilting angles perform in 2D beam-steering systems. The seminal journal paper on 2D Near-Field Meta-Steering has been limited to PGMs with a relatively smaller tilt angle of 20° [6]. They also require a lot of power to operate. For example, one commercial terminal with a fully electronic antenna system requires 0.6 kW peak (0.4 kW typical) power for 16 W Block Up Converter (BUC) and 0.5 kW peak (0.3 kW typical) power for 8 W BUC.

This work presents a two-step approach to reduce the dominant grating lobes and hence to enhance the pattern quality of Near-Field Meta-Steering systems. Firstly, we implement the Floquet space analysis on the periodically repeating pattern of the PGM to find the position and magnitude of dominant grating-type side lobes. A multi-objective particle swarm optimization (PSO) is used to reduce these lobes while simultaneously ensuring high transmission through every cell in the metasurface. Secondly, we investigate the performance of 2D Near-Field Meta-Steering systems for different transmission phase gradients in PGMs. We show that the number of dominant lobes in the far field are significantly reduced by increasing the slope of the near-field phase distribution at the output of a PGM.

To demonstrate the new approach, we have designed two Near-Field Meta-Steering systems. The first system consists of a pair of PGMs that have a smaller transmission phase gradient and each of the PGMs tilts an otherwise normal beam by 22°. The second system has a pair of metasurfaces with a larger transmission phase gradient, and each of these PGMs can individually tilt a normal beam by 30°. The radiation performance of the two systems are compared over a range of beam directions when the beam is steered in both elevation and azimuth planes.

The remaining manuscript is organized as follows. Section II explains the study performed on periodic supercells to predict and improve the performance of a complete near-field PGM, including supercell optimization. In Section II, 1D and 2D Near-Field Meta-Steering systems are designed and compared, and the results are discussed in detail in Section III. Section IV provides the concluding remarks.

II. Method

A. Phase-Transforming Cell

The phase-transforming cells (PTCs) are the fundamental components of phase-gradient metasurfaces that control the spatial phase variation of the electric field passing through them. The generic configuration of the PTCs is of immense importance because it determines the maximum phase range together with high transmission magnitude that can be achieved. Hence, a hybrid cell configuration with different metal patch shapes was carefully chosen after investigating several different cell configurations. The proposed cell family with a combination of circular and square printed metal patches, shown in Fig. 1, outperformed the cell family with patches that are all square and the cell family with patches that are all circular.

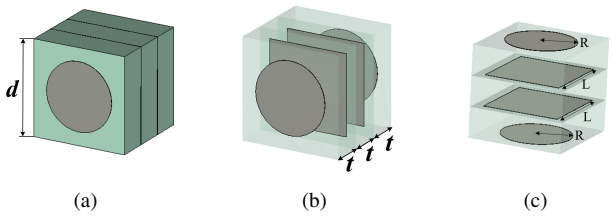

Fig. 1. Phase-transforming cell configuration: (a) one multi-layer phase-transforming cell (perspective view), (b) internal configuration of a cell showing metal patches on three layers of dielectric, (c) internal configuration of a cell showing two circular and two square metal patches (side-view).

Due to the existence of 90° rotational symmetry in both square and circular patches, the selected cell family is polarization independent [24]. Each cell has three dielectric layers of Taconic TLY-5 ($\epsilon_r = 2.2$) having the same thickness (t) of 1.5 mm (= $\lambda_\circ/10$), which are sandwiched between four metal patterns printed on dielectric. The dielectric material and thickness were selected after a parametric analysis such that they ensure high transmission for all phase shift values required, and the final metasurface is reasonably thin. The length of the square PTC (d) is $\lambda_\circ/3$ (5 mm @ 20 GHz), where $\lambda_\circ$ is the free-space wavelength at the operating frequency. It is pertinent to mention here that smaller cells reduce the phase quantization error [25]–[27], but they are incapable of providing sufficient transmission phase range while maintaining a transmission magnitude greater than -1 dB.

To elaborate this point further, the transmission and reflection characteristics of the PTC configuration shown in Fig. 1 were investigated for two lateral dimensions: $\lambda_\circ/3$ and $\lambda_\circ/4$. The two cell types were simulated in CST MWS using

periodic boundary conditions. The transmission phases and corresponding magnitudes for the two cell types were obtained by sweeping the sizes of metallic patches from minimum to maximum and stored in two separate databases. The phase values for the two cell types were normalized so that a PTC with no patches (i.e. all dielectric, $R = L = 0$) produces 0° normalized phase shift. Then, those two sets of data were used to find the dimensions of the patches that would produce the phase shift required for an actual beam-tilting metasurface at each location. It is well-known that in order to obtain a beam tilt of θ° in a 1D array, the progressive phase delay $\Delta\phi$ required between adjacent elements is given by [28], [29]:

$$\Delta\phi = \frac{2\pi}{\lambda_\circ} d \sin\theta \tag{1}$$

where d is the center to center spacing between adjacent cells and θ is the desired beam tilt. Thus, to tilt an otherwise normal beam by 30°, a metasurface requires a progressive phase shift ($\Delta\phi$) of 60° between adjacent cells when cell length (d) is $\lambda_\circ/3$ and a shift of 45° when cell length is $\lambda_\circ/4$. As the phase can be wrapped after completing a cycle of 360°, the number of unique cells (n) required to cover a complete cycle of 360° in the PGM can be calculated using $n = 2\pi/\Delta\phi$. For the two cases considered here, it is 6 and 8, respectively.

TABLE I
TRANSMISSION CHARACTERISTICS OF THE UNIQUE CELLS OF SIZES $d = \lambda_\circ/3$ AND $d = \lambda_\circ/4$ REQUIRED TO TILT A NORMAL BEAM BY 30°.

Cell Size (d)	$\Delta\phi$ (°)	Ideal Phase shift (ϕ_i°)	Available Phase shift (ϕ_i°)	Transmission Magnitude (dB)	Reflection Magnitude (dB)
$\lambda_\circ/3$	60	0	0	-0.02	-22.83
		60	60	-0.36	-10.99
		120	120	-0.44	-10.07
		180	180	-0.17	-14.06
		240	236	-0.14	-14.86
		300	298	-0.008	-27.27
$\lambda_\circ/4$	45	0	0	-0.02	-22.83
		45	45	-0.69	-8.31
		90	91	-1.37	-5.67
		135	140	-0.20	-6.02
		180	178	-0.30	-13.32
		225	220	-1.81	-4.65
		270	273	-0.99	-6.88
		315	326	-0.34	-11.23

Table I shows the unique phase values (ϕ_i°), here $i = 1, 2, ..., n$, ideally required to design the two PGMs for 2D beam steering, along with the corresponding closest phase shifts available in the database of the two cell types considered here. The table also gives the corresponding available transmission and reflection magnitudes for both cell types. It is evident form the table that the smaller ($\lambda_\circ/4$) cell type has a larger average phase error (i.e. the difference between the ideal phase shift and available phase shift), and transmission magnitude of some cells are less than -1 dB. The transmission and reflection magnitudes are very critical for near-field phase transformation metasurfaces because they are to be placed in a close proximity to the base antenna. For this reason, the larger ($\lambda_\circ/3$) cell type is preferred as it has smaller phase errors, higher transmission magnitudes ($>$ -0.5 dB) and negligible reflections ($<$ -10 dB) for all the required phase values.

B. Correlation Between Supercell Floquet Modes and the Dominant Grating Lobes in the Far-Field Pattern

A supercell, in the context of this paper, is an array of unique PTCs arranged in such a way that the transmission phase shift increases linearly [30]. Supercells are arranged periodically to form a full PGM and thus can be considered as the unit cell of this 2D periodic structure that is the metasurface. Since adjacent cells are different along the axis of increasing phase shift, the metasurface is not periodic at the cell scale but it is periodic at the supercell scale. To design a supercell that transforms a nearly uniform near-field phase at the input of the metasurface to a linearly increasing phase at its output, we combined six $\lambda_\circ/3$ cells from Table I. The configuration of the supercell is illustrated in Fig. 2. Such a supercell tilts the output beam to an offset angle of 30°.

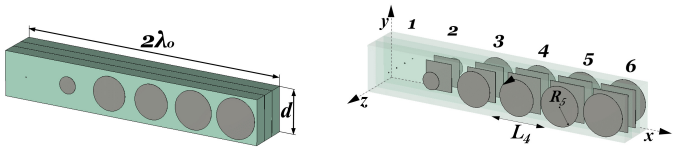

(a) (b)

Fig. 2. Supercell configuration: (a) a perspective view showing top metal layer and dielectric layers in a super cell, (b) internal configuration of the supercell, showing metal patches on four layers.

To analyze the performance of this supercell in a full metasurface, it was simulated in CST MWS under periodic boundary conditions with Floquet port excitation. For this numerical investigation, the supercell was excited with a broadside TE(00) mode propagating along the z-axis. Floquet analysis reveals that this supercell with a periodicity of $2\lambda_\circ$ supports 10 propagating TE modes out of which 5 are transmitting and 5 are reflecting. Then, for a finite-aperture metasurface, formed by cascading 8 such supercells along the x-axis, the far-field pattern was calculated using the array far-field calculator, which applies pattern multiplication to the far field of a single supercell. As illustrated in Fig. 3,

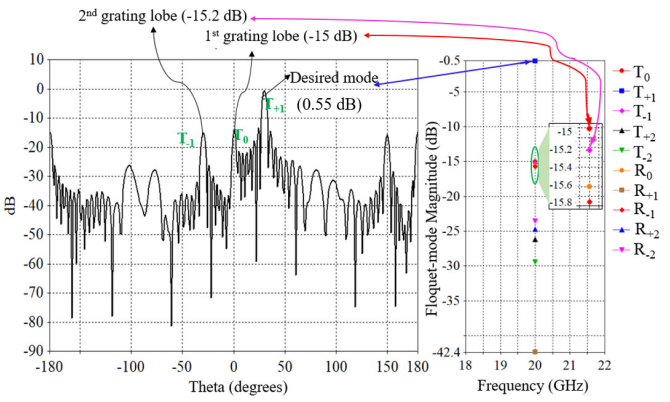

Fig. 3. Correlation between the supercell modes and the far-field pattern of a metasurface when the input field of the metasurface has uniform phase and amplitude.

excellent correlation is observed between the magnitudes and directions of the Floquet space modes predicted for an infinite

metasurface using the Floquet analysis and magnitudes and directions of the lobes in the far-field pattern obtained using the supercell simulation together with array calculation.

Floquet space analysis of this initial supercell does indicate that in the transmission region only three propagating modes are significant and the rest are evanescent. Among the transmitting modes, the space harmonic $m = +1$ corresponds to the desired beam at 30°, whereas $m = 0$ and $m = 1$ correspond to the two major grating lobes at 0° and −30°, respectively. Floquet space analysis accurately predicted the positions and relative magnitudes of the desired beam and grating lobes in the far field. This provides us with an opportunity to optimize the radiation pattern of a Near-Field Meta-Steering system using Floquet analysis, by selectively reducing the magnitudes of these "offending" modes that correspond to the strong grating lobes, very efficiently without carrying out extremely demanding simulations of the entire antenna and two metasurfaces.

C. Effect of Transmission Phase Gradient of a Near-Field PGM on Far-Field Pattern Lobes

Since the number of unique PTCs required to form a supercell is given by $n = 2\pi/\Delta\phi$, for a physically realizable metasurface design $\Delta\phi$ should preferably be a factor of 2π. In order to understand the relationship between the transmission phase gradient of a PGM and the nature of its far-field radiation pattern, we designed three supercells using $\lambda_\circ/3$ PTCs, and the design parameters obtained using eq. (1) are listed in Table II. The patch dimensions of each set of cells

TABLE II
THREE SUPERCELLS PRODUCING DIFFERENT BEAM TILT

$\Delta\phi$ (*in radians*)	Number of cells (n)	Beam-tilt $\theta_{out}(^\circ)$ for $\theta_{in} = 0^\circ$	Supercell length (textitd)
$\pi/3$	6	30	$6 \times \lambda_\circ/3 = 2\lambda_\circ$
$\pi/4$	8	22	$8 \times \lambda_\circ/3 = 8\lambda_\circ/3$
$\pi/5$	9	19.5	$9 \times \lambda_\circ/3 = 3\lambda_\circ$

with n = 6, 8 and 9 were selected from our pre-calculated databases, to achieve the desired phase values with high transmission magnitudes and low/near-zero reflections. These cells were then combined together in a similar way as shown in Fig. 2 to form three different supercells. They were simulated in CST MWS under periodic boundary conditions with Floquet port excitation. The radiation pattern was obtained by applying pattern multiplication on the far field of each supercell using array calculator in CST. From the results given in Fig. 4 we observe that the number of lobes in the visible range (−90° to +90°) of the far-field pattern decreases with the increase of gradient of the near-field phase at the supercell output. The beam tilt angle is proportional to the phase gradient. For a transmission phase gradient of 30°, there are three significant lobes among which the main lobe is at 30° and the two undesired major grating lobes are at 0° and −30°. The supercell with a transmission phase slope of 22° produces the main beam at 22° along with three strong grating lobes at −22°, 0° and 49°. However, for a slope of 19.5°, the main lobe is at 19.5° as expected, while the number of significant

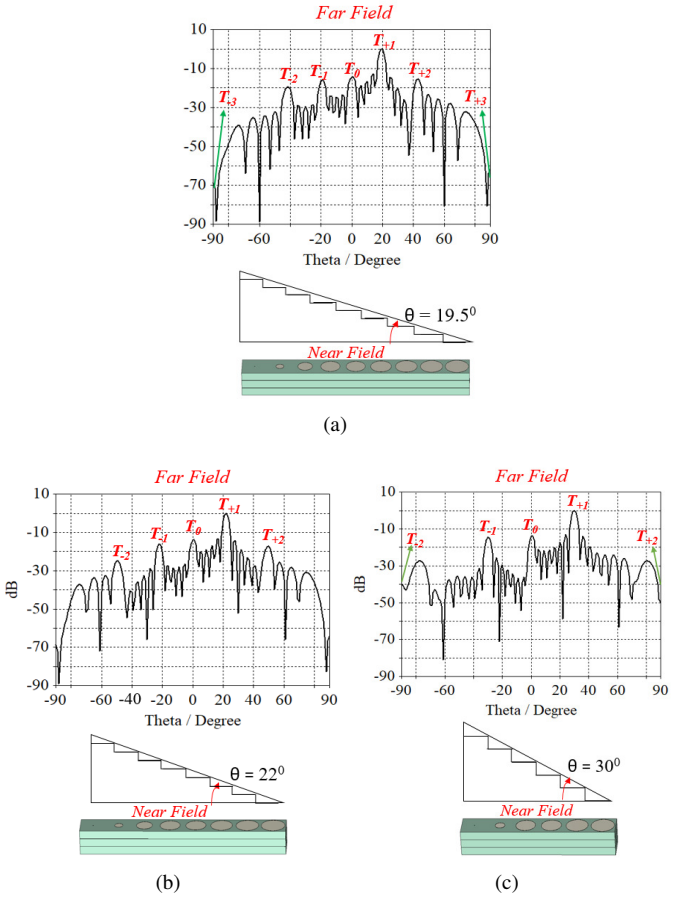

Fig. 4. The effect of near-field phase slope on far-field lobes. Near-field phase distribution and far-field radiation pattern for a supercell of length: (a) $(\lambda_\circ/3 \times 9 = 3\lambda_\circ)$, (b) $(\lambda_\circ/3 \times 8 = 8\lambda_\circ/3)$, (c) $(\lambda_\circ/3 \times 6 = 2\lambda_\circ)$.

grating lobes increases to four, occurring at −41°, −19°, 0° and 42° and all of them are above −25 dB. Thus, it is clear from Fig. 4 that steeper transmission phase gradient of the metasurface produces less number of lobes in the radiation pattern.

The physics behind the proposed methodology can be understood using the analytical theory of optical diffraction grating derived for far-field situation which is well described in the literature and pictorially illustrated in [31], [32]. According to this theory, the number of transmitted diffraction orders are governed by:

$$\sin\theta_m + \sin\theta_i = m\lambda/d, \tag{2}$$

where θ_m is the angle of diffraction, θ_i is the angle of incidence, m is the order of diffraction, λ is the wavelength and d is the period of the grating. For an optical grating with a normally propagating input, the grating equation can further be simplified to:

$$\sin\theta_m = m\lambda/d \tag{3}$$

The spurious diffraction modes in the visible region or upper hemisphere are observed until $\theta_m = 90^\circ$, i.e. $m\lambda/d \leq 1$ or $m \leq d/\lambda$. Hence, in a grating, the number of propagating modes is directly proportional to periodicity d. For $d = 2\lambda$,

there are five propagating modes for m = 0, ±1 and ±2, and for $d = 3\lambda$ there exist seven propagating modes for m = 0, ±1, ±2, ±3. Thus, diffraction theory confirms that in the far-field scenario also, a grating with a smaller period yields fewer number of diffracted modes. For a PTC of given dimensions, the size of the supercell or periodicity (d) depends on the slope of the transmission phase gradient of the PGM, as shown in Fig. 4. Supercell of a PGM is equivalent to one period of a diffraction grating. The steeper phase-gradient metasurface is similar to an optical grating with a smaller grating period and leads to a smaller number of transmission modes.

To further illustrate this analogy, the locations of diffracting modes calculated from analytical eq. (3) are superimposed on those obtained from electromagnetic simulations in Fig. 4. For d = $3\lambda_\circ$ the propagating modes $m = 0$, ±1, ±2 and ±3 are located at $0°$, $\pm19.5°$, $\pm41.81°$ and $\pm90°$, respectively. These locations were calculated using eq. (3) and shown in Fig. 4(a). Similarly, for $d = 8\lambda_\circ/3$ the propagating modes in the visible region, $m = 0$, ±1 and ±2 are located at $0°$, $\pm22°$ and $\pm48.5°$, respectively (Fig. 4(b)). For d = $3\lambda_\circ$, modes $m = 0, \pm1$ and ±2 are located at $0°$, $\pm30°$ and $\pm90°$, respectively (Fig. 4(c)). A previous analysis of the number and angular locations of propagating modes for diffraction gratings of different periodicity and orientation using a direction cosine diagram have reached the same conclusion [31]. Hence, to enhance the radiation pattern quality of a Near-Field Meta-Steering system, it is desirable to reduce the number and the strength of undesired grating lobes by increasing the transmission phase gradient of the PGM. To compare the performance of Near-Field Meta-Steering systems with different near-field phase gradients, let us proceed with $30°$ and $22°$ supercells.

D. Grating Lobe Reduction Using Floquet Space Optimization Approach

The existence of strong correlation between the magnitudes and directions of grating lobes in the far-field patterns of a practical PGM of finite size and the magnitudes and directions of corresponding supercell modes has been demonstrated previously in this paper (Fig. 3). Based on this correlation, we improve the radiation pattern of a finite-size metasurface by selectively reducing the magnitudes of stronger supercell modes that contribute to the worst grating lobes. It was observed that both $22°$ and $30°$ supercells support 10 propagating modes for transmission and reflection. We use the particle swarm optimization (PSO) algorithm in CST to optimize the dimensions of each metal patch R_n and L_n, where $n = 1, 2, 3...i$. Here, R is the radius of the circular patch, and L is the length of the square patch in each cell of the supercell (Fig. 2 (b)). The objective of optimization is to bring all 9 undesired modes below -25 dB, while simultaneously maintaining the desired mode above -0.1 dB. The goal (FF) was formulated as a weighted sum of two aforementioned objectives as below:

$$FF = [w_m\{\max(0, (-0.1 - DM))\}]^2 + \quad (4)$$

$$\sum_{i=1}^{9}[w_i\{\max(0, (UDM - (-25)))\}]^2, \quad (5)$$

where $w_m = 9$, which is the weight defined to increase the transmission magnitude of the desired mode (DM), and w_i are the weights for undesired modes (UDM) defined based on the strength of their magnitudes and can take the values from 1 to 9. They are higher for most dominant modes and lower for the other modes. In order to ease the search process of the PSO algorithm, the patch dimensions obtained from our databases were provided as an initial seed for optimization. The algorithm was allowed to run until all the lobes were below -22 dB. It was observed that beyond this point the fitness function did not improve for 30 consecutive runs and algorithm was stopped manually.

TABLE III
DIMENSIONS OF SUPERCELLS (mm)

Transmission phase gradient of Supercell (°)	Initial Dimensions (mm)		Optimized Dimensions (mm)	
30	L1 = 0.1	R1 = 0.05	L1 = 0.09	R1 = 0.05
	L2 = 3	R2 = 0.95	L2 = 2.99	R2 = 0.97
	L3 = 3.3	R3 = 1.9	L3 = 3.3	R3 = 1.9
	L4 = 3.8	R4 = 1.95	L4 = 3.5	R4 = 1.99
	L5 = 3.9	R5 = 2.15	L5 = 3.85	R5 = 2.14
	L6 = 4	R6 = 2.25	L6 = 4.1	R6 = 2.22
22	L1 = 0.1	R1 = 0.05	L1 = 0.09	R1 = 0.05
	L2 = 2.8	R2 = 0.8	L2 = 2.65	R6 = 0.84
	L3 = 3.1	R3 = 1.55	L3 = 2.85	R6 = 1.49
	L4 = 3.4	R4 = 1.95	L4 = 3.34	R6 = 1.98
	L5 = 3.8	R5 = 1.95	L5 = 3.74	R6 = 1.81
	L6 = 3.9	R6 = 2.1	L6 = 3.84	R6 = 2.05
	L7 = 4	R7 = 2.2	L7 = 3.92	R6 = 2.16
	L8 = 4	R8 = 2.3	L8 = 4.05	R6 = 2.3

Table III shows the dimension of the initial and optimized supercells for $22°$ and $30°$ beam-tilting metasurfaces. Six repetitions of a $22°$ supercell has the same aperture ($6\times8\times\lambda_\circ/3$) as eight repetitions of the $30°$ supercell. As before, CST array calculator was used to generate the far-field patterns of both $30°$ and $22°$ metasurfaces with 8 and 6 repetitions along the x-axis, respectively. The normalized far-field patterns for both the initial and optimized supercells are compared in Fig. 5. It can be noted that optimization has substantially

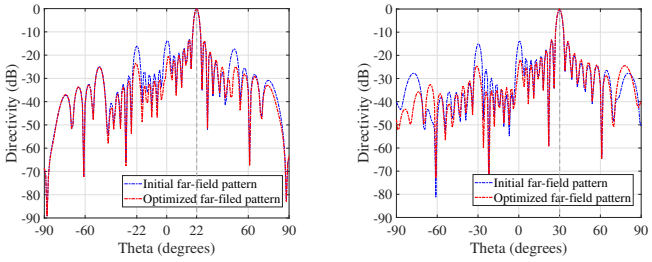

(a) (b)

Fig. 5. Comparison between initial and optimized far-field patterns for (a) a $22°$ beam-tilting metasurface and (b) a $30°$ beam-tilting metasurface illustrating the suppression of the stronger grating lobes.

reduced the strength of grating lobes. The most rewarding outcome is that, the optimization has successfully reduced the level of the most-significant undesired grating lobes in both metasurfaces to below -22 dB. Some of them were

greater than -15 dB in the initial design. Additionally, our optimization approach considers the model as a black box, and hence mutual coupling between individual elements (cells and patches) in each supercell and between the supercells are taken into account in our full-wave optimizations. Further, unlike in previous metasurface designs [6], the effects of the difference in size between adjacent patches in neighbouring cells on mutual coupling, is also accounted for in this method.

E. Correlation between Far Field of a Supercell and Far Field of a 2D Metasurface

It was shown in [18], [19] that a supercell simulation under periodic boundary conditions in the CST-MWS frequency-domain solver provides an accurate approximation of a full metasurface. However, simulating large and complex structures in this frequency-domain solver is time and memory consuming, while CST-MWS time-domain solver is more efficient for the analysis of electrically large beam-steering systems. The key difference between the two methods is that the latter takes into consideration any edge effect. Hence, it is desirable to compare the far-field patterns from supercell simulations with the far-field patterns obtained using the time-domain solver.

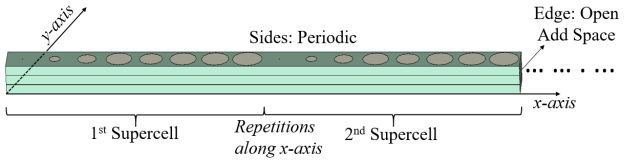

Fig. 6. 2D metasurface designed by finite repetitions of supercells along the x-axis.

For this purpose, we modelled a 2D metasurface by increasing the finite number of supercell repetitions along x-axis and periodic boundary along the y-axis. The metasurface was simulated with CST time-domain solver. The specified boundary conditions are shown in Fig 6. We refer to this structure as a 2D metasurface that is finite in x direction.

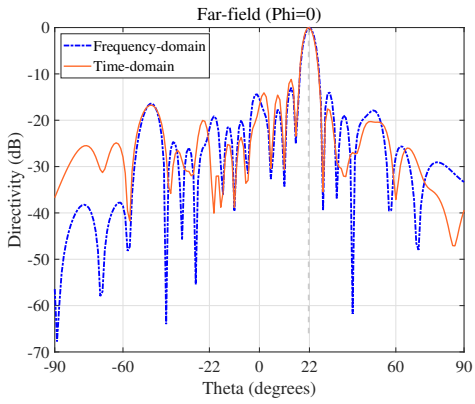

Fig. 7. Similarity between the far-field pattern of a 2D metasurface with 1D finiteness obtained from time-domain analysis and the far-field pattern of the same supercell array but without edge effects, obtained from frequency-domain analysis.

It was observed that the far-field radiation pattern of such a metasurface consisting of more than three supercells, when excited by a plane wave, shows a reasonable similarity with the far-field pattern predicted from supercell simulations. Fig. 7 compares the far-field pattern generated by a 2D metasurface designed using four repetitions of a supercell along x-axis in CST time-domain solver and the far field of the same supercell array calculated by specifying four repetitions in the array calculator. It is evident that similarity exists in terms of position of main beam and grating lobes. The difference is attributed to the fact that the supercell time-domain analysis results include the edge effects. Thus, a supercell in CST frequency-domain solver and a 2D metasurface in CST time-domain solver are good approximations for a full metasurface. The supercell serves as a simple and accurate model of a full metasurface when predicting radiation performance of a complex metasurface with a large aperture. Its optimization is a lot more efficient.

III. Implementation

A. 1D Beam-Steering System

As demonstrated above, four repetitions of a supercell along x-axis is sufficient to accurately predict the radiation pattern of a metasurface. Thus, we use the PSO-optimized supercells from Section II to design two complete PGMs for 30° and 22° beam tilting in the elevation plane. To design a PGM with a square aperture of $12\lambda_\circ \times 12\lambda_\circ$, the 30° supercell was repeated 6 times along the x-axis and 36 times along the y-axis. Similarly, for the same aperture size, the 22° supercell was repeated 4.5 times along the x-axis and 36 times along the y-axis. Note that if necessary, these PGMs can be cut into a circular aperture with a diameter equal to the side-

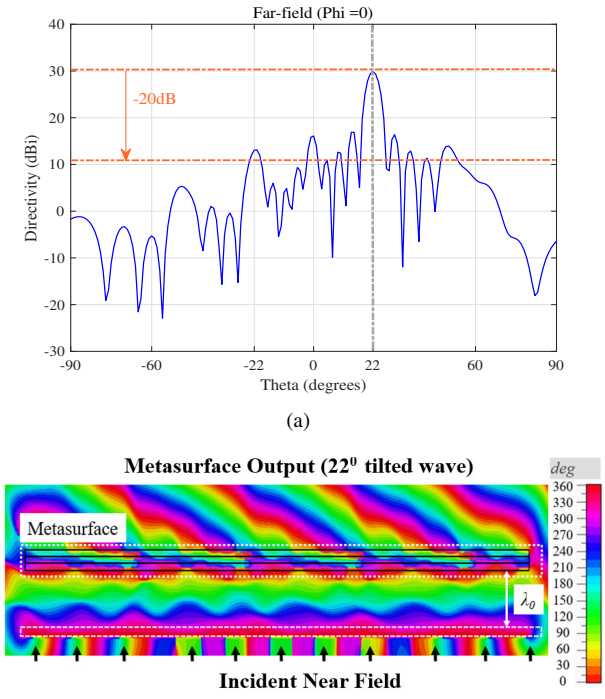

Fig. 8. 22° beam-steering metasurface: (a) far-field pattern and (b) near-field phase distribution when excited with a normally incident plane wave.

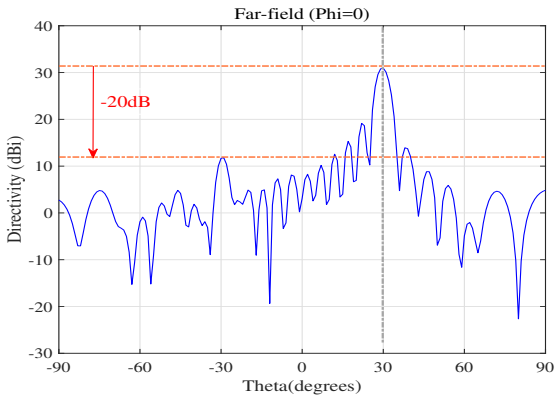

(a)

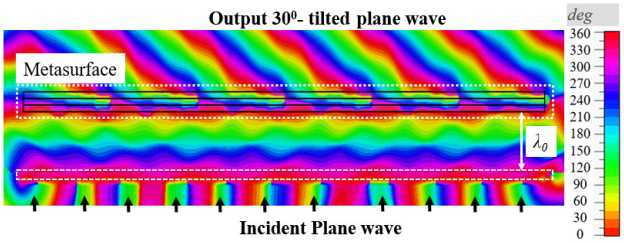

(b)

Fig. 9. 30° beam-steering metasurface: (a) far-field pattern and (b) near-field phase distribution when excited with a normally incident plane wave.

length of the metasurface, to avoid gain loss due to angular mismatch during beam-steering. Both PGMs were simulated in CST time-domain solver with a normally incident plane wave feed having the $\vec{E}$ field vector parallel to the *y*-axis. The open boundary conditions were specified along both *x* and *y*-axes. The near-field phase distribution and far-field radiation patterns of the two PGMs with $\delta = 22°$ and $\delta = 30°$ are shown in Fig. 8 and Fig. 9, respectively. We observe a smooth, nearly linear increase in the phase of the output. The beam-tilt angle (δ) in the far field is proportional to the slope of the output near-field phase of the PGM. Since the metasurface maintains a constant phase along the *y*-axis and varies it linearly along the *x*-axis, it essentially mimics the properties of dielectric wedges [6], [33]. Such a surface can be rotated about its axis to steer the output beam along the surface of a cone with a vertex angle of δ. We observe that the 22° PGM has three grating lobes above −20 dB (at +44°, 0° and −22°) but the 30° PGM has no grating lobes above −20 dB. For the same aperture the directivity of the 22° PGM is 29.9 dBi and that of 30° PGM is 31.4 dBi. The lesser directivity of 22° PGM is due to larger number and higher levels of grating lobes, both mean more energy being directed in the undesired directions.

B. 2D Beam-Steering System

The two PGMs, denoted by MS1 and MS2 in Fig. 10, are placed in close proximity and one above the other. The beam-tilt angles for MS1 and MS2 are δ_1 and δ_2, respectively. The symbols ψ_1 and ψ_2 denote the orientation angles of metasurfaces, which can be changed by rotating each metasurface individually around *z*-axis. It is assumed that the metasurface

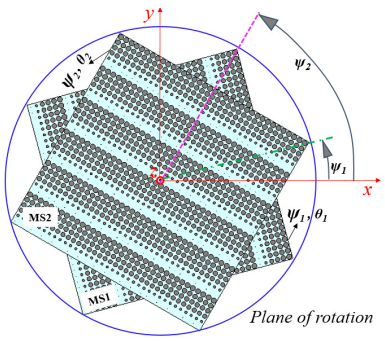

Fig. 10. A pair of metasurfaces, MS1 (bottom) and MS2 (top), for 2D beam-steering.

pair is excited using a high-gain aperture antenna such as a radial line slot array antenna, an array of resonant cavity antennas, a microstrip patch array or a metasurface antenna [34]–[37]. We also assume in this paper that the near-field phase distribution produced by the antenna is uniform but if it is not uniform then it can be corrected by modifying MS1 using the method described in [36]–[38]. The angular position of the beam in far field can be represented by a pair of angles (θ, ϕ) where θ is elevation angle (measured from the *z*-axis) and ϕ is the azimuth angle. The direction of the steered beam depends on δ_1, δ_2, ψ_1 and ψ_2. Since δ_1 and δ_2 are the properties of the metasurfaces, they are fixed for a given beam-steering system. Thus, ψ_1 and ψ_2 are varied to achieve full 2D beam steering.

We now describe the effect of ψ_1 and ψ_2 on the angular position of the main beam in a beam-steering system. Maximum tilt in the elevation angle (θ_{max}) is obtained when both MS1 and MS2 are aligned such that $\psi_1 = \psi_2$. When the orientations of the metasurfaces are such that $\psi_1 - \psi_2 = 180°$, θ is 0° and the beam is in the broadside direction provided that $\delta_1 = \delta_2$ (i.e. identical MS1 and MS2). Rotating only one MS while keeping the other fixed moves the beam in both elevation and azimuth planes. If $\psi_1 = 0$ and ψ_2 is varied from 0° to 180°, the azimuth angle increases according to $\phi = \psi/2$, while the elevation angle gradually decreases to 0°. Further increase of ψ_2 from 180° to 360° will gradually increase elevation angle back to θ_{max}. When both MSs are synchronously co-rotated (same angle in same direction), the azimuth angle (ϕ) changes while the the elevation angle θ remains unchanged. When the two surfaces are synchronously counter-rotated (same angle in opposite direction), the beam moves only in the elevation plane while ϕ remains unchanged. The complete process of steering has been pictorially elaborated in [6].

To investigate the effects of variation of phase gradient of PGMs on the steering performance of 2D beam-steering systems, we designed two different steering systems as in Fig. 10, one with a pair of 22° PGMs and the other with a pair of 30° PGMs. For brevity, the scanning system with two 22° PGMs will hereby be referred to as System-I, and the other system will be referred to as System-II. In both cases, the separation between the two PGMs is $\lambda_\circ$. In order to move the beam in both azimuth and elevation plane, MS1 was fixed at $\psi_1 = 0$ and MS2 was rotated from $\psi_2 = 180°$ to $\psi_2 = 0°$

such that the beam tilt is increased in the elevation plane from $\theta = 0^\circ$ to $\theta = \theta_{max}$, with a step of 10°.

The far-field radiation pattern cuts taken at elevation planes where the beam peak exists in System-I and System-II are shown in Fig. 11 and Fig. 12, respectively. The highest directivity for System-I is noted when $\psi_2 = 180^\circ$ and it is equal to 30.5 dBi. For the same orientation ($\psi_2 = 180^\circ$), System-II has a peak directivity of 31.4 dBi, which is 0.9 dBi higher than System-I. It can be observed that the number and level of grating lobes are less in System-II. It can be clearly seen in both Fig. 11 and Fig. 12 that the peak directivity decreases when the main beam is tilted away from the broadside. The SLLs of System-I increases dramatically with steering in elevation plane, whereas in System-II the SLLs are below -19 dB for the all elevation plane pattern cuts.

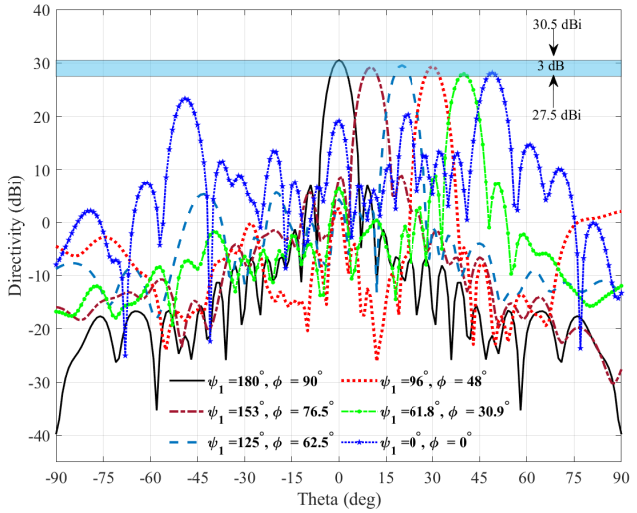

Fig. 11. Elevation plane radiation pattern cuts for each rotation of MS2 ($\psi_1 = 0$ and ψ_2 is varied) in System-I.

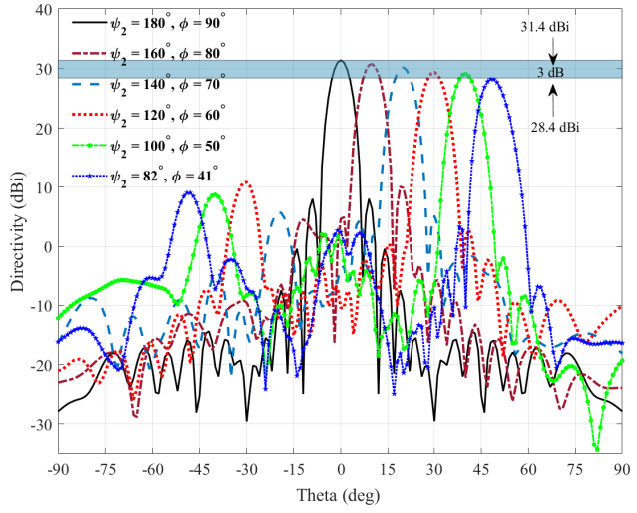

Fig. 12. Elevation plane radiation pattern cuts for each rotation of MS2 ($\psi_1 = 0$ and ψ_2 is varied) in System-II.

For further illustration, we compare the 2D far-field patterns of the two scanning systems as shown in Fig. 13. These contour plots show all lobes that are above -20 dB. The number of grating-type side-lobes above -20 dB (N), directivity (D) in dBi and orientation angle of rotating metasurface (ψ_2) for each system and for each beam tilt θ are listed in Table IV. It can be seen that for the same beam tilt θ, the number of grating-type side-lobes above -20 dB is more in System-I than in System-II. As a result, System-II has higher directivity compared to System-I for all beam directions. The beams can be moved up or down in 2-D plane in Fig. 13 by co-rotating the metasurfaces MS1 and MS2. Thus, it is clear that both the systems are capable of covering the elevation angles ranging from 0° to 48° and they can be mechanically rotated to achieve complete 2D steering covering a large cone with an apex angle of 96°. One important outcome of this comparative analysis is that it gives apriori knowledge to an antenna engineer to make a wise choice of metasurfaces when designing a 2D beam-steering system. Using steeper PGMs it is possible to achieve a specific 2D beam-steering range with less number of grating lobes, weaker grating-type side lobes and higher directivity.

TABLE IV
COMPARISON OF TWO DIFFERENT BEAM STEERING SYSTEMS

θ	System-I (*Two* 22° *PGMs*) $\psi_1 = 0^\circ$				System-II (*Two* 30° *PGMs*) $\psi_1 = 0^\circ$			
	ψ_2	ϕ	N	D (dBi)	ψ_2	ϕ	N	D (dBi)
0°	180°	90°	8	30.5	180°	90°	6	31.4
10°	153°	76.5°	12	29.2	160°	80°	5	30.8
20°	125°	62.5°	10	29.5	140°	70°	4	30.4
30°	96°	48°	12	29.3	120°	60°	7	29.4
40°	61.8°	30.9°	9	27.9	100°	50°	8	29.1
48°	0°	0°	16	28.1	82°	41°	8	28.2

To achieve elevation beam steering up to 48°, System-I needs to rotate MS2 all the way from 0° to 180° but System-II produces the same elevation tilt by rotating MS2 only from 82° to 180°. Thus System-II needs less rotation of MS2 compared to System-I for the same tilt. That means, for a given rotation mechanism, System-II will steer faster.

According to the Floquet-Bloch theorem, a Huygen's metasurface can be designed to transform a plane wave incident at an angle θ_{in} to a refracted plane wave at an angle θ_{out} by varying electric surface reactance and magnetic surface susceptance over a 2D planar surface [19]. If the same metasurfaces is excited by an incident wave propagating at an angle ψ_{in} where $\psi_{in} \neq \theta_{in}$, the nth mode transmitted plane wave output angle is given by:

$$\psi_n = arcsin(\sin\psi_{in} + n\Delta_{sin}) \tag{6}$$

where $\Delta_{sin} = \sin\theta_{out} - \sin\theta_{in}$. If a PGM is designed to transform a normally incident plane wave to a 22° tilted output plane wave by varying the phase shifts over a 2D plane, $\theta_{in} = 0^\circ$ and $\theta_{out} = 22^\circ$. Thus, for a normally incident plane wave feed, the first metasurface is excited at the designated incident angle and will produce an output plane wave tilted at an angle of 22°. The second metasurface placed above the first is excited with a wave that is already propagating at an angle (ψ_{in}) of 22°, where $\psi_{in} \neq \theta_{in}$ and hence is a non-designated incident angle. For System-I consisting of

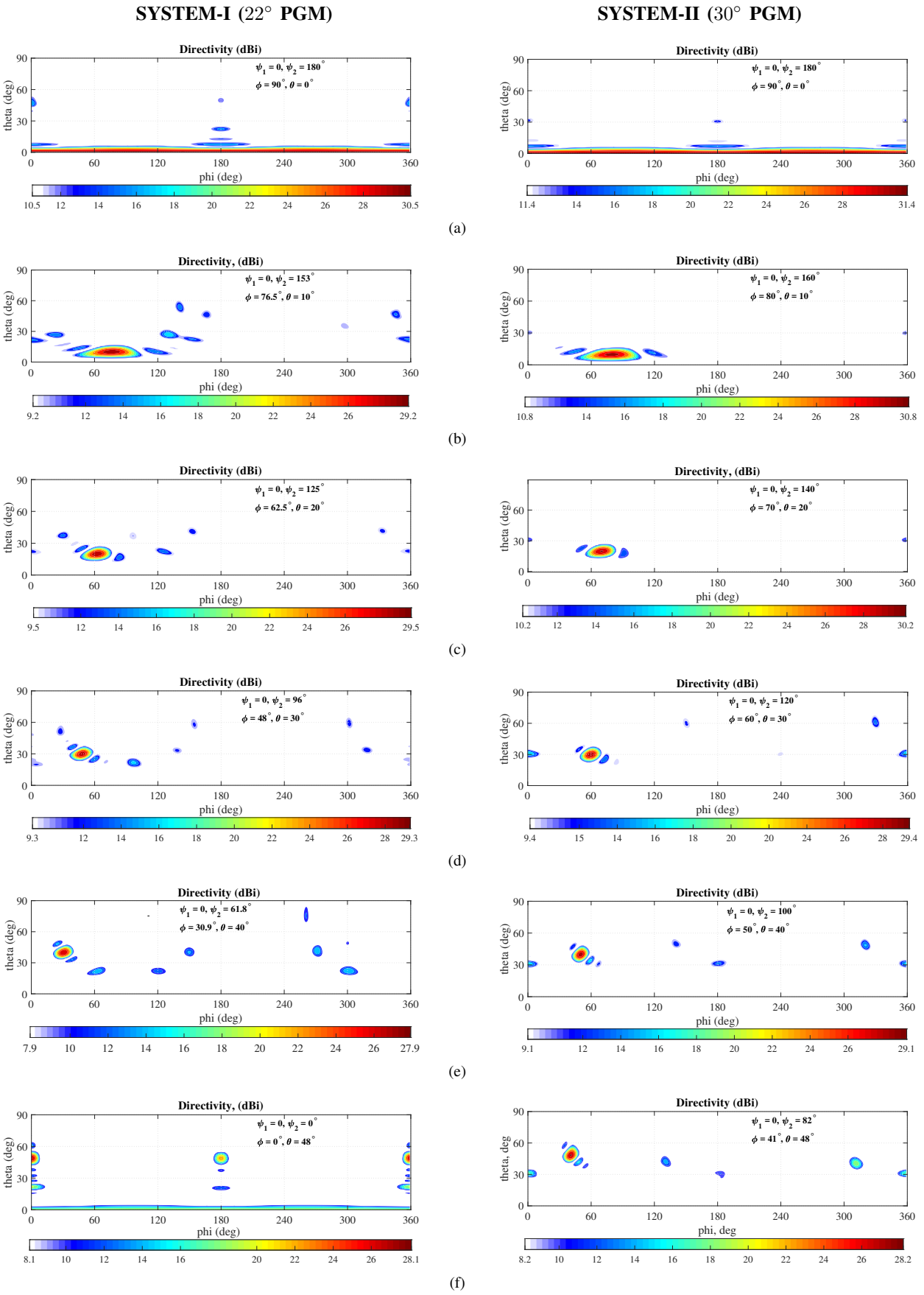

Fig. 13. 2D far-field patterns showing all grating lobes above -20 dB for System-I and System-II: (a) $\theta = 0°$, (b) $\theta = 10°$, (c) $\theta = 20°$, (d) $\theta = 30°$, (e) $\theta = 40°$, (f) $\theta = 48°$

two identical PGMs each with a tilt of 22°, the maximum elevation tilt possible, predicted by (6), is 48°. For System-II, the maximum theoretical elevation tilt given by (6) is 90°. However, in practice such extreme tilt is not achievable but a tilt greater than 48° is still possible in System-II. It is interesting to note that the decrease in directivity when the beam is tilted from $\theta = 0°$ to $\theta = 48°$ is 2.4 dB for System-I and 3.2 dB in System-II.

Another important factor that governs the utility of metasurfaces in Near-Field Meta-Steering is its loading effect on the base antenna. It has been mentioned in previous works [6], [39] that loading effect is critical and reflecting metasurfaces can have severe effect on antenna matching. However, if the spacing between antenna and metasurface is kept sufficiently larger ($> \lambda_\circ/2$) and the metasurface is optimized to have negligible reflections then the loading effect on the base antenna is negligible [40]. To validate this point a pair of metasurfaces aligned to direct the beam in broadside direction was excited using an array of Hertzian dipoles placed half a wavelength apart, with a PEC ground plane placed a quarter wavelength below the array. The distance between the base of metasurface pair and dipole array was varied between $\lambda_\circ/4$ to $\lambda_\circ$ to study the effect on radiation characteristics. All dipoles were fed with same amplitude and phase. The radiation patterns shown in Fig. 14, start to deteriorate when

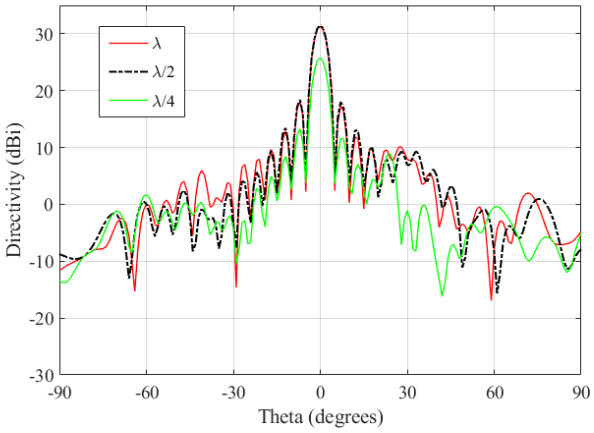

Fig. 14. Radiation patterns of System II aligned for broadside beam when excited with an array of Hertzian dipoles at distances varying from $\lambda_\circ/4$ to $\lambda_\circ$.

the gap is decreased below $\lambda_\circ/2$. Thus, in this case, the distance between the base antenna and the lowest metasurface should at least be $\lambda_\circ/2$. This simulation includes the effect of non-near-plane-wave components of incident field and there is no significant effect on overall performance of the steering system. It should be noted that this is the worst case (largest minimum separation required) we came across in all related research projects conducted by the authors and others in our research group. In [6] where the base antenna is a Fabry-Perot resonant cavity antenna, the gap between the top surface of the base antenna and the lower surface of the metasurface pair was $8mm$ ($< \lambda_\circ/3$ @ 11GHz) and in more recent projects where the base antenna was a horn antenna the minimum gap required was zero but a fraction of a millimeter was allowed in the prototype to allow easy rotation of the metasurfaces without touching the base antenna [41].

The near-field PGMs can be placed in the close proximity of the base antenna ($> \lambda_\circ/2$) as well as close to each other when designing a Near-Field Meta-Steering system. This is due to the fact that these PGMs have insignificant mutual coupling since they are highly transparent. To demonstrate this, the radiation pattern of System-II was studied by varying the distance between two metasurfaces between $\lambda_\circ$ and $\lambda_\circ/8$. The radiation patterns for different spacing values between the metasurfaces were compared in Figs. 15 and 16 for two different metasurface orientations, which produce a broadside beam and a 20° tilted beam, respectively. The pattern shows

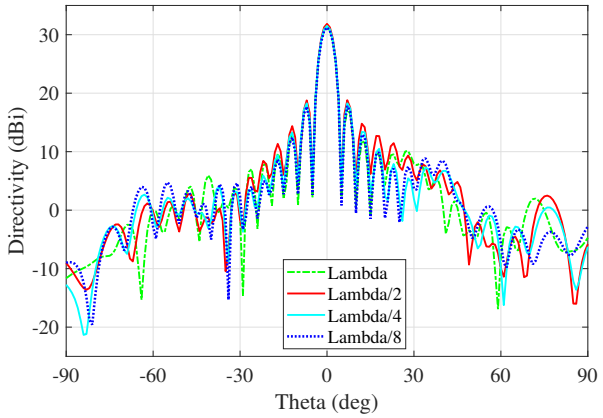

Fig. 15. Radiation patterns of System II aligned for broadside beam, for different spacing between the pair of metasurfaces ranging from $\lambda_\circ/8$ to $\lambda_\circ$ when excited with a normally incident plane wave.

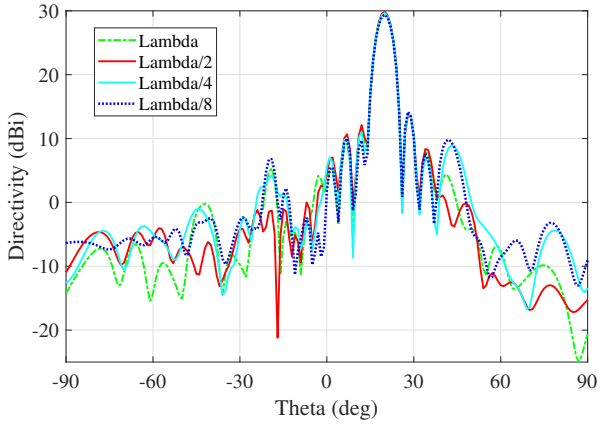

Fig. 16. Radiation patterns of System II aligned for 20° beam tilt, for different spacing between the pair of metasurfaces ranging from $\lambda_\circ/8$ to $\lambda_\circ$ when excited with a normally incident plane wave.

almost negligible variations in the main lobe and major side lobes with changing distance between the two metasurfaces. Therefore, these PGMs can be placed as close as $\lambda_\circ/8$ with no significant effect on directivity and side lobes. Although a full -wave simulation cannot model every practical issue associated with prototyping, these numerical results confirm

that this method can be applied to mitigate significantly the grating-lobe challenge in Near-Field Meta-Steering.

To compare the performance of a Near-Field Meta-Steering system with a fixed beam base antenna having no metasurface at all, an array of Hertzian dipoles was simulated with a PEC ground plane placed a quarter wavelength below the array. The peak directivity of the array is 32.5 dBi at 20 GHz. A 1D Near-Field Meta-Steering system formed by placing one 30° PGM half a wavelength above this dipole array shows a directivity reduction of 1 dB with a peak directivity of 31.5 dBi. This reduction can be attributed partly to the non-plane wave propagating component from the array and partly to the scattering caused by the metasurface when placed in the near field of the antenna. The directivity of the corresponding 2D Near-Field Meta-Steering system formed by placing a second PGM half a wavelength above the first, at an orientation angle of 180°, is 31.3 dBi. The total drop in directivity due to both PGMs is only 1.2 dB. The directivity patterns for the three cases are shown in Fig. 17.

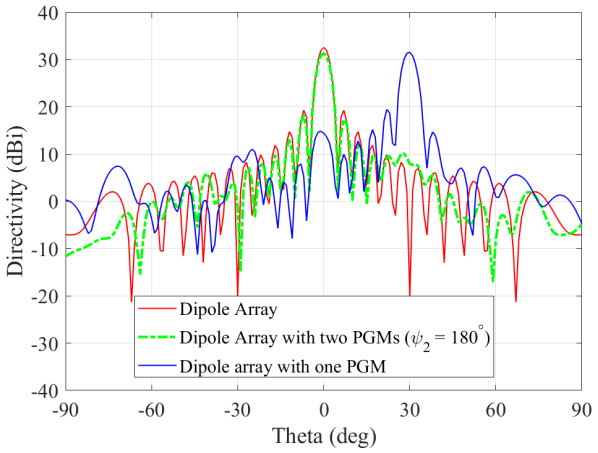

Fig. 17. Radiation pattern of System II when excited with an array of Hertzian dipoles.

The bandwidth of directivity is yet another important figure of any antenna system [42], [43]. Although the metasurfaces were designed in this work to function in one frequency, information transfer in a practical system requires certain bandwidth. Thus, it is desirable to investigate directivity bandwidth of the system, considering the fact that phase gradients of the surfaces can change with frequency. To explore the bandwidth of System-II with respect to steering angle, the radiation characteristics were investigated over a frequency band of 2 GHz centered around 20 GHz. When the two metasurfaces are aligned such that the beam is in the broadside direction, the system exhibits highest directivity of 31.6 dBi from 20.2 GHz to 20.3 GHz and 1dB directivity bandwidth of 1 GHz (from 19.6 GHz to 20.6 GHz). From 19 GHz to 21 GHz, the maximum variation in directivity is 2.3 dB. Thus, 3dB directivity bandwidth is greater than 2 GHz for this orientation. However, when the orientation of metasurfaces is varied such that the main beam is tilted to 20°, the system has highest directivity of 30.2 dBi from 20 GHz to 20.2 GHz and lowest directivity of 28.5 dBi at 19 GHz. 1dB directivity bandwidth of the system is 1 GHz from 19.4 GHz to 20.4 GHz within which it produces the expected beam steering of 20°. The 3dB directivity bandwidth may still be greater than 2 GHz. It was noted that the 3dB beamwidth of the Near-Field Meta-Steering system changes slightly with frequency, especially when the beam is steered to large tilt angles. When tilted to a nominal angle of 20°, the 3dB beamwidths at 19 GHz, 20 GHz and 21 GHz are 17.5° to 24°, 16.8° to 22.9° and 15.9° to 21.80°, respectively. Lastly, when the tilt angle is 35° this Meta-steering system has a maximum directivity of 29.6 dBi from 20.3 GHz to 20.6 GHz, its 1dB directivity bandwidth is 0.6 GHz from 19.6 GHz to 20.1 GHz and its 3dB beamwidths at 19 GHz, 20 GHz and 21 GHz are 33.2° to 40.4°, 31.6° to 38.1° and 30.1° to 36.2°, respectively.

IV. Conclusion

A Floquet space analysis of a supercell was performed, and it revealed excellent correlation between the magnitudes and the directions of the Floquet modes and the most dominant grating lobes in the far-field pattern of a PGM. This fact was further exploited with a multi-objective optimization to reduce the levels of the strongest grating lobes in the farfield of a metasurface used for beam-steering. Our optimization takes into account the variations in mutual coupling between dissimilar adjacent cells in a supercell. When steering or tilting the beam of a high-gain antenna using a near-field PGM, undesirable grating lobes are often noted. In general, optimization of an electrically large metasurface to control these “offending” grating lobes for every beam direction is computationally exhaustive and challenging. In particular, optimization of a 2D Near-Field Meta-Steering system consisting of two near-field PGMs is extremely challenging due to small metallic features in these large structures. Thus, the proposed approach is efficient and useful for controlling the SLLs of such systems. Just by optimizing a simpler and smaller supercell, this approach saves a great deal of computation power, resources and time.

The radiation pattern quality of several near-field PGMs are compared for different gradients of transmission phase. It is found that the steeper the transmission phase slope, the lesser are the number and the significance of the dominant grating lobes in the far field. Two different beam-steering systems were designed using PGMs with different transmission phase gradients, and their beam-steering performance figures are compared. The scanning system with larger-gradient PGMs exhibits better performance for all steering angles in both planes, with less number of significant grating lobes, weaker grating lobes and higher directivity. It requires less mechanical rotation of metasurfaces to achieve the same beam tilt from the normal direction and hence the beam steering is faster. Unlike in previously published work [6] and [8], this paper successfully addresses the issue of high SLLs and simultaneously maintains high directivity while performing beam steering.

It has been shown that the gap between the two metasurfaces in a Near-Field Meta-Steering system can be decreased to $1/8$ of a wavelength with no significant effect on the radiation pattern quality. The minimum gap between the base antenna

and the metasurface pair in a 2D Near-Field Meta-Steering system depends on the type of the antenna. Previously, with a resonant cavity base antenna, this was as short as $8mm$ ($\approx \lambda_\circ/3$) at 11 GHZ [6]. It was noted here that for an array of dipoles with a PEC ground plane, a gap of around half a wavelength is suitable.

ACKNOWLEDGMENT

The authors would like to thank the Guest Editors Professors Ashwin K. Iyer, Andrea Alu and Ariel Epstein for inviting Professor Esselle to contribute this paper to the Special Issue on Recent Advances in Metamaterials and Metasurfaces. The authors acknowledge the support from the Australian Research Council (ARC) discovery grant to K.P. Esselle and Australian government international Research Training Pathway (iRTP) scholarship to K. Singh.

REFERENCES

[1] J. Duggan, *Adaptive beamforming with a focal-fed offset parabolic reflector antenna.* Queen's University at Kingston, 1998.

[2] A. W. Rudge and M. J. Withers, "New technique for beam steering with fixed parabolic reflectors," *Proceedings of the Institution of Electrical Engineers*, vol. 118, no. 7, pp. 857–863, July 1971.

[3] https://www.emsolutions.com.au/products-and-solutions/cotm?id=66.

[4] M. Maddocks and M. Smith, "A steerable flat-plate antenna design for satellite communications and broadcast reception," in *1989 Sixth International Conference on Antennas and Propagation, ICAP 89 (Conf. Publ. No. 301)*. IET, 1989, pp. 40–44.

[5] S. B. C. William W. Milroy, "Variable inclination continuous transverse stub array," Nov. 3 2003, pub. No. US 2004/0233117 A1. [Online]. Available: https://patents.google.com/patent/US6919854B2/en

[6] M. U. Afzal and K. P. Esselle, "Steering the beam of medium-to-high gain antennas using near-field phase transformation," *IEEE Transactions on Antennas and Propagation*, vol. 65, no. 4, pp. 1680–1690, 2017.

[7] ——, "High-gain beam steering by near-field phase transformation-an overview," in *2018 IEEE International Symposium on Antennas and Propagation & USNC/URSI National Radio Science Meeting*. IEEE, 2018, pp. 1447–1448.

[8] N. Gagnon and A. Petosa, "Using rotatable planar phase shifting surfaces to steer a high-gain beam," *IEEE Transactions on Antennas and Propagation*, vol. 61, no. 6, pp. 3086–3092, 2013.

[9] Y. Yang, "Analytic solution of free space optical beam steering using risley prisms," *Journal of Lightwave Technology*, vol. 26, no. 21, pp. 3576–3583, 2008.

[10] H. D. Griffiths and M. R. Khan, "Antenna beam steering technique using dielectric wedges," *IEE Proceedings H - Microwaves, Antennas and Propagation*, vol. 136, no. 2, pp. 126–131, April 1989.

[11] Y. Lu, Y. Zhou, M. Hei, and D. Fan, "Theoretical and experimental determination of steering mechanism for risley prism systems," *Applied optics*, vol. 52, no. 7, pp. 1389–1398, 2013.

[12] Y. Hou, L. Chang, Y. Li, Z. Zhang, and Z. Feng, "Linear multibeam transmitarray based on the sliding aperture technique," *IEEE Transactions on Antennas and Propagation*, vol. 66, no. 8, pp. 3948–3958, 2018.

[13] S. A. Matos, E. B. Lima, J. S. Silva, J. R. Costa, C. A. Fernandes, N. J. Fonseca, and J. R. Mosig, "High gain dual-band beam-steering transmit array for satcom terminals at ka-band," *IEEE Transactions on Antennas and Propagation*, vol. 65, no. 7, pp. 3528–3539, 2017.

[14] https://spacenews.com/panasonic-avionics-jurys-still-out-on-profitability-of-in-flight-connectivity/ .

[15] A. A. Artemenko and R. O. Maslennikov, "Electronically beam-steerable antenna device," Mar. 7 2017, uS Patent 9,590,300.

[16] A. A. Artemenko, V. N. Ssorin, R. O. Maslennikov, and A. V. Mozharovskiy, "Lens antenna with electronic beam steering capabilities," Apr. 30 2015, uS Patent App. 14/593,552.

[17] S. Chen, D. K. Karmokar, Z. Li, P. Qin, R. W. Ziolkowski, and Y. J. Guo, "Continuous beam scanning at a fixed frequency with a composite right/left-handed leaky-wave antenna operating over a wide frequency band," *IEEE Transactions on Antennas and Propagation*, pp. 1–1, 2019.

[18] G. Lavigne, K. Achouri, V. S. Asadchy, S. A. Tretyakov, and C. Caloz, "Susceptibility derivation and experimental demonstration of refracting metasurfaces without spurious diffraction," *IEEE Transactions on Antennas and Propagation*, vol. 66, no. 3, pp. 1321–1330, March 2018.

[19] M. Chen, E. Abdo-Sánchez, A. Epstein, and G. V. Eleftheriades, "Theory, design, and experimental verification of a reflectionless bianisotropic huygens' metasurface for wide-angle refraction," *Physical Review B*, vol. 97, no. 12, p. 125433, 2018.

[20] L. Zhang, R. Y. Wu, G. D. Bai, H. T. Wu, Q. Ma, X. Q. Chen, and T. J. Cui, "Transmission-reflection-integrated multifunctional coding metasurface for full-space controls of electromagnetic waves," *Advanced Functional Materials*, vol. 28, no. 33, p. 1802205, 2018.

[21] H. Li, G. Wang, T. Cai, J. Liang, and X. Gao, "Phase- and amplitude-control metasurfaces for antenna main-lobe and sidelobe manipulations," *IEEE Transactions on Antennas and Propagation*, vol. 66, no. 10, pp. 5121–5129, Oct 2018.

[22] M. Boyarsky, M. F. Imani, and D. R. Smith, "Grating lobe suppression in metasurface antenna arrays with a waveguide feed layer," *arXiv preprint arXiv:1905.09846*, 2019.

[23] L. Zhang, X. Wan, S. Liu, J. Y. Yin, Q. Zhang, H. T. Wu, and T. J. Cui, "Realization of low scattering for a high-gain fabryperot antenna using coding metasurface," *IEEE Transactions on Antennas and Propagation*, vol. 65, no. 7, pp. 3374–3383, July 2017.

[24] N. Gagnon, A. Petosa, and D. A. Mcnamara, "Thin microwave phase-shifting surface lens antenna made of square elements," *Electronics Letters*, vol. 46, no. 5, pp. 327–329, March 2010.

[25] N. Gagnon, A. Petosa, and D. A. McNamara, "Research and development on phase-shifting surfaces (psss)," *IEEE Antennas and Propagation Magazine*, vol. 55, no. 2, pp. 29–48, April 2013.

[26] H. Nematollahi, J. Laurin, J. E. Page, and J. A. Encinar, "Design of broadband transmitarray unit cells with comparative study of different numbers of layers," *IEEE Transactions on Antennas and Propagation*, vol. 63, no. 4, pp. 1473–1481, April 2015.

[27] A. H. Abdelrahman, A. Z. Elsherbeni, and F. Yang, "Transmission phase limit of multilayer frequency-selective surfaces for transmitarray designs," *IEEE Transactions on Antennas and Propagation*, vol. 62, no. 2, pp. 690–697, Feb 2014.

[28] N. Gagnon, A. Petosa, and D. A. McNamara, "Thin phase-correcting lens antennas made using a three-layer phase-shifting surface (pss) at ka band," in *2010 14th International Symposium on Antenna Technology and Applied Electromagnetics the American Electromagnetics Conference*, July 2010, pp. 1–4.

[29] T. Hongnara, S. Chaimool, P. Akkaraekthalin, and Y. Zhao, "Design of compact beam-steering antennas using a metasurface formed by uniform square rings," *IEEE Access*, vol. 6, pp. 9420–9429, 2018.

[30] Achouri, Karim, Khan, Bakthiar Ali, Gupta, Shulabh, Lavigne, Guillaume, Salem, Mohamed Ahmed, and Caloz, Christophe, "Synthesis of electromagnetic metasurfaces: principles and illustrations," *EPJ Applied Metamaterials*, vol. 2, p. 12, 2015. [Online]. Available: https://doi.org/10.1051/epjam/2015016

[31] J. E. Harvey and C. L. Vernold, "Description of diffraction grating behavior in direction cosine space," *Applied optics*, vol. 37, no. 34, pp. 8158–8159, 1998.

[32] F. D. Tart and J. E. Harvey, "Alignment theory and practice for diffraction grating rhombs," in *Optical alignment II*, vol. 483. International Society for Optics and Photonics, 1984, pp. 2–9.

[33] H. D. Griffiths and M. R. Khan, "Antenna beam steering technique using dielectric wedges," *IEE Proceedings H - Microwaves, Antennas and Propagation*, vol. 136, no. 2, pp. 126–131, April 1989.

[34] G. Minatti, S. Maci, P. De Vita, A. Freni, and M. Sabbadini, "A circularly-polarized isoflux antenna based on anisotropic metasurface," *IEEE Transactions on Antennas and Propagation*, vol. 60, no. 11, pp. 4998–5009, 2012.

[35] M. Bosiljevac, M. Casaletti, F. Caminita, Z. Sipus, and S. Maci, "Non-uniform metasurface luneburg lens antenna design," *IEEE transactions on antennas and propagation*, vol. 60, no. 9, pp. 4065–4073, 2012.

[36] A. Lalbakhsh, M. U. Afzal, K. P. Esselle, S. L. Smith, and B. A. Zeb, "Single-dielectric wideband partially reflecting surface with variable reflection components for realization of a compact high-gain resonant cavity antenna," *IEEE Transactions on Antennas and Propagation*, vol. 67, no. 3, pp. 1916–1921, March 2019.

[37] A. Lalbakhsh, M. U. Afzal, K. P. Esselle, and S. L. Smith, "Wideband near-field correction of a fabryperot resonator antenna," *IEEE Transactions on Antennas and Propagation*, vol. 67, no. 3, pp. 1975–1980, March 2019.

[38] M. U. Afzal and K. P. Esselle, "A low-profile printed planar phase correcting surface to improve directive radiation characteristics of

electromagnetic band gap resonator antennas," *IEEE Transactions on Antennas and Propagation*, vol. 64, no. 1, pp. 276–280, Jan 2016.
[39] A. Kiyani, K. P. Esselle, M. U. Afzal, L. Matekovits, and R. M. Hashmi, "A low-profile phase correcting solution to improve directivity of horn antenna," in *2018 International Conference on Electromagnetics in Advanced Applications (ICEAA)*, Sep. 2018, pp. 332–333.
[40] X. Zhao, C. Yuan, L. Liu, S. Peng, Q. Zhang, L. Yu, and Y. Sun, "All-metal beam steering lens antenna for high power microwave applications," *IEEE Transactions on Antennas and Propagation*, vol. 65, no. 12, pp. 7340–7344, Dec 2017.
[41] A. A. Baba, R. M. Hashmi, K. P. Esselle, J. G. Marin, and J. Hesselbarth, "Broadband partially reflecting superstrate-based antenna for 60 ghz applications," *IEEE Transactions on Antennas and Propagation*, vol. 67, no. 7, pp. 4854–4859, July 2019.
[42] G. Minatti, M. Faenzi, M. Sabbadini, and S. Maci, "Bandwidth of gain in metasurface antennas," *IEEE Transactions on Antennas and Propagation*, vol. 65, no. 6, pp. 2836–2842, June 2017.
[43] G. Wu, S. Qu, and S. Yang, "Wide-angle beam-scanning reflectarray with mechanical steering," *IEEE Transactions on Antennas and Propagation*, vol. 66, no. 1, pp. 172–181, Jan 2018.

Khushboo Singh (S'17) received B.Tech degree in electronics and communication engineering from SHIATS, Allahabad, India, in 2012 and M.S. by Research degree in electronics and communication engineering from LNMIIT, Jaipur, India, in 2014. She is currently pursuing the Ph.D. degree with the Centre for Collaboration in Electromagnetic and Antenna Engineering (C4CELANE), Macquarie University, Sydney, NSW, Australia.

From 2014-2015, she was an assistant professor in the department of Electronics and Communication Engineering, PITS, Sikar, India. From 2015 to 2016 she was a guest lecturer in the department of electronics and communication engineering, SRHU, Dehradun, India. Her research interests include, antenna arrays, phase-gradient metasurfaces, high-gain planar metasurface based antennas, evolutionary optimization methods in electromagnetics and surface electromagnetics, waveguide polarizers and couplers.

Khushboo has received LNMIIT merit based scholarship during her master studies. She is a recipient of prestigious Australian government funded iRTP scholarship for Ph.D.

Muhamamd U. Afzal (S'13–M'16) received the B.S. degree in electronics engineering (hons.) and Masters degree in Computational Science and Engineering from National University of Sciences and Technology (NUST), Islamabad, Pakistan, in 2005 and 2011, respectively. He completed his PhD in electronics engineering from Macquarie University in 2016.

From 2010 to 2012, he was a lab engineer at Samar Mubarakmand Research Institute of Microwave and Millimeter-wave Studies (SMRIMMS), Islamabad, Pakistan. From 2012 to 2013, he was a lecturer in the electrical engineering department, NUST, Islamabad, Pakistan. He is now a research associate at Macquarie University, engineering department. His research interests include electromagnetic band gap or Fabry-Perot resonator antennas, high-gain planar metasurface based antennas, radial-line slot antennas, phased arrays, free-standing phase-shifting structures or metasurfaces, frequency selective surfaces, near-field phase transformation, and far-field pattern synthesis using near-field phase transformation.

Mr. Muhammad received NUST merit base scholarship during undergraduate studies and International Macquarie Research Excellence Scholarship (iMQRES) for PhD studies.

Maria Kovaleva (S'14) received B.S. degree in electrical engineering (Hons) from Moscow Technical University of Communications and Informatics (MTUCI), Russia, in 2011, and Ph.D. degree (VC commend.) from Macquarie University, Australia. She is currently an Associate Lecturer at Curtin University, Australia.

She was an Antenna Design Engineer with the JSC NIIKP (Russian Space Systems), Moscow, Russia from 2011 to 2014, and a Postdoctoral Research Associate at the Centre for Collaboration in Electromagnetic and Antenna Engineering (C4CELANE), Sydney, Australia from 2017 to 2019. Her research interests include aperture arrays, antennas for radio astronomy, microwave and millimetre-wave antennas, resonant cavity antennas, evolutionary optimization methods in electromagnetics and surface electromagnetics.

Professor Karu Esselle IEEE M (1992), SM (1996), F (2016), is the Distinguished Professor in Electromagnetic Antenna Engineering at the University of Technology Sydney and a Visiting Professor of Macquarie University, Sydney. According to a Special Report published by The Australian national newspaper in 2019, he is the National Research Field Leader in Microelectronics and Electronic Packaging fields in Engineering Discipline as well as the Electromagnetism field in the Disciplines of Physics and Mathematics.

Karu received BSc degree in electronic and telecommunication engineering with First Class Honours from the University of Moratuwa, Sri Lanka, and MASc and PhD degrees with near-perfect GPA in electrical engineering from the University of Ottawa, Canada. Previously he was Director of WiMed Research Centre and Associate Dean Higher Degree Research (HDR) of the Division of Information and Communication Sciences and directed the Centre for Collaboration in Electromagnetic and Antenna Engineering at Macquarie University. He has also served as a member of the Deans Advisory Council and the Division Executive and as the Head of the Department several times.

In 2018 and again in 2019, Karu has been selected to chair the prestigious Distinguished Lecturer Program Committee of the IEEE Antennas and Propagation (AP) Society the premier global learned society dedicated for antennas and propagation - which has about 9,000 members worldwide. After two stages in the selection process, Karu was also selected by this Society as one of two candidates in the ballot for 2019 President of the Society. Only three people from Asia or Pacific apparently have received this honour in the 68-year history of this Society. Karu is also one of the three Distinguished Lecturers (DL) selected by the Society in 2016. He is the only Australian to chair the AP DL Program ever, the only Australian AP DL in almost two decades, and second Australian AP DL ever (after UTS Distinguished Visiting Professor Trevor Bird). He has been continuously serving the IEEE AP Society Administrative Committee in several elected or ex-officio positions since 2015. Karu is also the Chair of the Board of management of Australian Antenna Measurement Facility, and was the elected Chair of both IEEE New South Wales (NSW), and IEEE NSW AP/MTT Chapter, in 2016 and 2017. Karu was elevated to prestigious IEEE Fellow grade for his contributions to resonance-based antennas. He is also a Fellow of Engineers Australia.

Karu has authored approximately 600 research publications and his papers have been cited over 8,400 times. In 2018 alone his publications received 1084 citations. He is the first Australian antenna researcher ever to reach Google Scholar h-index of 30 and his citation indices have been among the top Australian antenna researchers for a long time (in October 2019: i10 is 164 and h-index is 43). Since 2002, his research team has been involved with research grants, contracts and PhD scholarships worth over 18 million dollars, including 15 Australian Research Council grants, without counting the 245 million-dollar SmartSat Corporative Research Centre, which started in 2019. His research has been supported by many national and international organisations including Australian Research Council, Intel, US Air Force, Cisco Systems, Hewlett-Packard, Australian Department of Defence, Australian Department of industry, and German and Indian governments.

Karus awards include 2019 Motohisa Kanda Award (from IEEE USA) for the most cited paper in IEEE Transactions on EMC in the past five years, selection as a Finalist for the forthcoming 2019 Macquarie University Research Excellence Awards for Innovative Technologies, 2019 ARC Discovery International Award, 2017 Excellence in Research Award from the Faculty of Science and Engineering, 2017 Engineering Excellence Award for Best Innovation, 2017 Highly Commended Research Excellence Award from Macquarie University, 2017 Certificate of Recognition from IEEE Region 10, 2016 and 2012 Engineering Excellence Awards for Best Published Paper from IESL NSW Chapter, 2011 Outstanding Branch Counsellor Award from IEEE headquarters (USA), 2009 Vice Chancellors Award for Excellence in Higher Degree Research Supervision and 2004 Innovation Award for best invention disclosure. His mentees have been awarded many fellowships, awards and prizes for their research achievements. Forty-eight international experts who examined the theses of his recent PhD graduates ranked them in the top 5 to 10 percent.

Karu has provided expert assistance to more than a dozen companies including Intel, Hewlett Packard Laboratory (USA), Cisco Systems (USA), Audacy (USA), Cochlear, Optus, ResMed and Katherine-Werke (Germany). Among them, his team designed the high-gain antenna system for the worlds first entirely Ka-band CubeSat made by Audacy, USA and launched to space by SpaceX in December 2018. This is believed to be the first Australian-designed high-gain antenna system in space, since CSIRO-designed antennas in Australias own FedSat launched in 2002.

Karu is in the College of Expert Reviewers of the European Science Foundation (2019-22) and he has been invited to serve as an international expert/research grant assessor by several other research funding bodies as well, including European Research Council and national agencies in the Netherlands, Canada, Finland, Hong-Kong, Georgia, South Africa and Chile. He has been invited by Vice-Chancellors of Australian and overseas universities to assess applications for promotion to professorial levels. He has also been invited to assess grant applications submitted to Australias most prestigious schemes such as Australian Federation Fellowships and Australian Laureate Fellowships. In addition to the large number of invited conference speeches he has given, he has been an invited keynote speaker of several IEEE and URSI conferences and workshops including URSI19 Seville, Spain, and 23rd ICECOM in 2019 in Dubrovnik, Croatia.

He is an Associate Editor of IEEE Transactions on Antennas Propagation as well as IEEE Access. He is the Technical Program Committee Co-Chair of ISAP 2015, APMC 2011 and TENCON 2013 and the Publicity Chair of ICEAA 2016, IWAT 2014 and APMC 2000. His previous research activities are posted in the web at http://web.science.mq.edu.au/ esselle/ .